Size-Controlled Self-Assembly of Anisotropic Sepiolite Fibers in Rubber Nanocomposites

Barbara Di Credico,[a,*] *Elkid Cobani,*[1] *Emanuela Callone,*[b] *Lucia Conzatti,*[c] *Davide Cristofori,*[d] *Massimiliano D'Arienzo,*[a] *Sandra Dirè,*[b] *Luca Giannini,*[e] *Thomas Hanel,*[e] *Roberto Scotti,*[a] *Paola Stagnaro,*[c] *Luciano Tadiello,*[e] *Franca Morazzoni*[a]

[a] Dept. of Materials Science, INSTM, University of Milano-Bicocca, Via R. Cozzi, 55, 20125 Milano, Italy. Tel: +39-02-64485023; e-mail: barbara.dicredico@unimib.it

[b] "K. Müller" Magnetic Resonance Lab., Dept. of Industrial Engineering, University of Trento, Via Sommarive, 9, 38123 Trento, Italy.

[c] Istituto per lo Studio delle Macromolecole, ISMAC, CNR, Via De Marini 6, 16149 Genova, Italy

[d] Dipartimento di Scienze Molecolari e Nanosistemi, Università Ca' Foscari Venezia and Centro di Microscopia Elettronica "G. Stevanato" Via Torino 155/b, 30172 Venezia-Mestre, Italy

[e] Pirelli Tyre SpA, Viale Sarca, 222, 20126 Milano, Italy

Abstract

The development of advanced polymer nanocomposites requires a strong filler-polymer interfacial interaction and an optimal filler nanodispersion. The incorporation of the clays into a polymer matrix frequently does not improve the composite mechanical properties, owing to both poor dispersion and macroscopic particle dimensions. In this work, pristine and organically-modified sepiolites (Sep) were structurally modified by an acid treatment, which provides nano-sized sepiolite (NS-Sep) fibers with reduced particle size and increased silanol groups on the surface layer. NS-Sep fibers were used to prepare styrene-butadiene rubber nanocomposites.

Dynamic-mechanical analysis of clay polymer nanocomposites demonstrated that the NS-Sep fibers provided an excellent balance between reinforcing and hysteretic behaviour, compared to the large-sized pristine Sep and isotropic silica. This was related to the enhanced interfacial chemical interaction between NS-Sep and rubber, as well as to the size and self-assembly of anisotropic nanofibers to form filler network structures, as supported by transmission electron microscopy analysis.

The preparation of nanocomposites, based on Sep nanofibers obtained by a simple and versatile acid treatment, can thus be considered a new approach for the designing of advanced clay polymer nanocomposites.

KEYWORDS clay nanocomposite; sepiolite; self-assembly.

1. Introduction

Mechanical properties of rubber based materials critically depend on vulcanization (Susanna et al., 2016; Scotti et al., 2015) and addition of reinforcing fillers (Sabu et al., 2010; Heinrich et al., 2012). The most widely used fillers are carbon black and silica, although in the last decades clay fillers consisting of two-dimensional layers with plate-like geometry, *e.g.* talc, mica, or layered silicates, have been frequently considered as promising candidates for the strengthening of various types of polymer matrices (Krishnamoorti et al., 1996; Alexandre et al., 2000).

It is commonly accepted that, beside the hydrodynamic effect due to filler volume fraction, the reinforcement mechanism consists of two main contributions (Kraus 1965; Frolich et al., 2005). The first one is related to the *filler network structure*, and contributes to the total modulus together with the polymer network (Vilgis et al., 2009). The rationale of this is that, in a given range of particle loading, the filler gives rise to interconnected structures, through both the direct particles interaction, and their bridging by polymer chains (Kluppel et al., 1997). In this respect, the size and shape of the filler have a pronounced significance. In fact it is clearly demonstrated that the reinforcing effect varies with the particle shape (Donnet and Custoder, 2005). Specifically, clay fillers have reinforcing effect higher than spherical ones, due to the high aspect ratio (AR) of the lamellar particles having layers approximately of 1 nm thickness and 1000 nm length (Galimberti, 2011). The second contribution is associated to the *interfacial interaction* between filler and polymer, which induces the slowing down of the chain mobility, increasing the fraction of the polymer rigid phase (Dutta et al., 1994). Recently, our group reported that rod-like silica particles with high AR (*i.e.* 2–7) provide significant rubber reinforcement (Scotti et al., 2014; Tadiello et al., 2015) thanks to the self-alignment of the anisotropic particles and to the consequent increased filler/polymer interface. These results suggest the possibility of tuning the

formation of the filler network improving the filler-rubber interaction by using high AR fillers, like clays. These latter are of high applicative interest because they are environmental friendly, naturally occurring and readily available in large quantities at lower cost compared to other fillers.

Unfortunately, the incorporation of clays into a polymer matrix frequently does not improve the composite mechanical properties as sought after (Bandyopadhyay et al., 2006). This is basically due to the poor dispersion aptitude of the clay minerals because of the low affinity between the *inorganic* layers and the *organic* polymer. Thus, a modification of the filler surface is required to favor the *interfacial interactions*. To this aim, the hydrophilic pristine clays are generally modified by organic molecules (typically cationic surfactants), *via* ion exchange reaction (Kojima et al., 1993; Li et al., 2008) or by grafting reaction with silane-based coupling agents (Herrera et al., 2005; Yang et al., 2012).

It might also be noted also that clay fillers have dimensions in macroscopic scale. This may be a drawback, considering that, keeping constant the filler content, nano-sized particles with high surface area lead instead to very wide filler-matrix interfaces, modifying the molecular mobility of polymer chains and thus inducing a significant reinforcing effect. However, up to now the preparation of clay-based rubber composites still employs particles with dimensions of many micro-meters, which might not fully exfoliate during mixing. To face with this issue, several research groups have performed chemical modifications of specific clays (Ruiz-Hitzky and Meerbeek, 2006), but only few ones managed to decrease their average size toward the nanometric scale (Zha et al., 2014).

Among clays, sepiolite (Sep) has attracted researcher attention because of its easy availability, low cost, high specific surface area, strong mechanical and chemical stability, and anisotropic particle shape (Miles, 2011). Sep is a 2:1 phyllosilicate with formula [$Si_{12}O_{30}$ Mg_8 $(OH)_4(OH_2)_4 \cdot nH_2O$] (Murray 2007). It has rather unusual structure, organized in two-dimensional silica tetrahedral sheets including one central magnesium octahedral sheet, continuous in one direction. In the third direction, sheets have a thickness of about 1.34 nm and share each edge with the neighboring one, producing a “checkerboard” type pattern. As the sheets are covalently bonded they cannot be exfoliated. The Sep elemental particle appears as tiny fibers 40-150 nm width and 1-10 μm length. Fibers usually stick together in bundles having 0.1 to 1 μm diameter. The bundles form randomly-

oriented aggregates having size ranging 10-100 μm. The breaking down of these almost tightly packed aggregates is still a challenge for scientists, if they want to take advantage of the peculiar Sep shape for designing nanostructured materials. Several applications of Sep-based hybrid materials have been proposed in literature, *e.g.* for removing pollutants from the water or for obtaining artificial bones (Ruiz-Hitzky et al., 2010; Galan, 2011). In elastomer formulation instead, the use of pristine Sep is very limited due to its hydrophilic surface and to the consequent low affinity towards organic polymers. On the other hand, even if the organically-modified Sep clays result more easily dispersible in a polymer matrix, the polymer-filler interaction is generally not improved (Gonzalez Hernandez et al., 1987). Meanwhile, surface treatment *via* silane coupling agent is poorly effective, consisting only in 10% of functionalized sepiolite (Nahmias Nanni et al., 2012).

In this paper, for the first time, we report a new approach to prepare rubber nanocomposites based on *size-controlled* Sep *nanofibers*, obtained by applying a controlled surface treatment on bare Sep. In detail, moving from the literature methods (Aznar et al., 1992; Valentin et al., 2006 and 2007; Esteban-Cubillo et al., 2008), a simple acid treatment was employed. This provides needle-shaped Sep fibers with nanometric size (namely nano-sized Sep, NS-Sep), preserving the filler anisotropic features and increasing the amount of bonding sites at the Sep edge surfaces. The simultaneous silanization reaction of Sep surface, during acid treatment, was also investigated by using tri-functional silane coupling agent. Morphological, spectroscopic and thermal analyses were performed for a complete characterization of the modified Sep clays. These were used to prepare styrene-butadiene rubber (SBR) nanocomposites by *ex-situ* blending. The filler-filler and filler-rubber interactions were investigated through dynamic-mechanical tests and by assessing the NS-Sep nanocomposite structure by transmission electron microscopy (TEM) analysis. The size and the self-assembly ability of the anisotropic NS-Sep nanofibers seem to be critical to form filler network structures, which are able to attain a better balance of the reinforcing and hysteretic properties, in comparison to those obtained by using pristine Sep and conventional nanosilica.

To the best of our knowledge, this is the first example of advantageous use of Sep nanofibers, as low hysteresis reinforcing filler in elastomers.

2. Experimental Section

2.1 Materials

Sep Pangel S9 (SepS9) and the organically modified Sep Pangel B5 (SepB5, organically-modified with *N*,*N*-didodecyl-*N*-methyl-ammonium, DDMA) were supplied by Tolsa and extracted from the landfill of Vallecas (Spain). Silica Zeosil MP1165 (BET specific surface area 160 m^2g^{-1}) was from Solvay. Bis(3-triethoxysilylpropyl) tetrasulfide (TESPT), ammonium hydroxide, isopropanol (iPr-OH) and 37% aqueous hydrocloric acid were purchased from Sigma-Aldrich. Deionized water and aqueous ammonium hydroxide (60%) were used during washing procedures. Milli-Q water was used with a resistivity 18.2 MΩ cm.

Compounding: SBR was SLR 4630 from Styron Europe GmbH (25% styrene; 63% vinyl; 12% butadiene); Treated Distillate Aromatic Extract (TDAE) extender oil (37.5 parts per hundred rubber (phr)); *N*-(1,3-dimethylbutyl)-*N'*-phenyl-*p*-phenylendiamine (6PPD) used as antidegradant was Santoflex-6PPD from Flexsys; stearic acid was Stearina TP8 from Undesa; sulfur was from Zolfoindustria; zinc oxide was from Zincol Ossidi; *N*-cyclohexyl-2-benzothiazole sulfenamide (CBS) was Vulkacit CZ/C from Lanxess: N-tert-butyl-2-benzothiazyl sulfenamide. Technical Compounding: (high-cis neodymium polybutadiene rubber (BR) was Europrene 40 from Versalis; synthetic polyisoprene (IR) was SKI3 from produced by Nitzhnekamsk); Carbon Black N550 was from Cabot; *N-tert*-butyl-2-benzothiazyl sulfenamide (TBBS) from Lanxess; polymerized 2,2,4-trimethyl-1,2-dihydroquinoline (TMQ) was from General Quimica S.A.

2.2 Acid treatment of SepS9 and SepB5

SepX (with X = S9 or B5, 120.0 g) was suspended in iPr-OH (1.2 L) at 65 °C and vigorously stirred (800 revolutions per minute (rpm)) for 30 min. Then 37% aqueous HCl solution (480 mL) was added to the reaction mixture. The reaction mixture was stirred at 65 °C (600 rpm) for 2 h, and then filtered. The resulting solid was washed repeatedly with distilled deionized water and with aqueous ammonium hydroxide (60%) until pH 7± 0.2. Finally, the powder was filtered, washed again with distilled water (until no chloride anions were detected by AgCl precipitation) and dried in an oven at 120 °C for 48 h. The obtained product was labeled NS-SepX.

Scheme 1 (synthetic pathway with H^+) illustrates the changes in the SepX structure after the above described acid treatment.

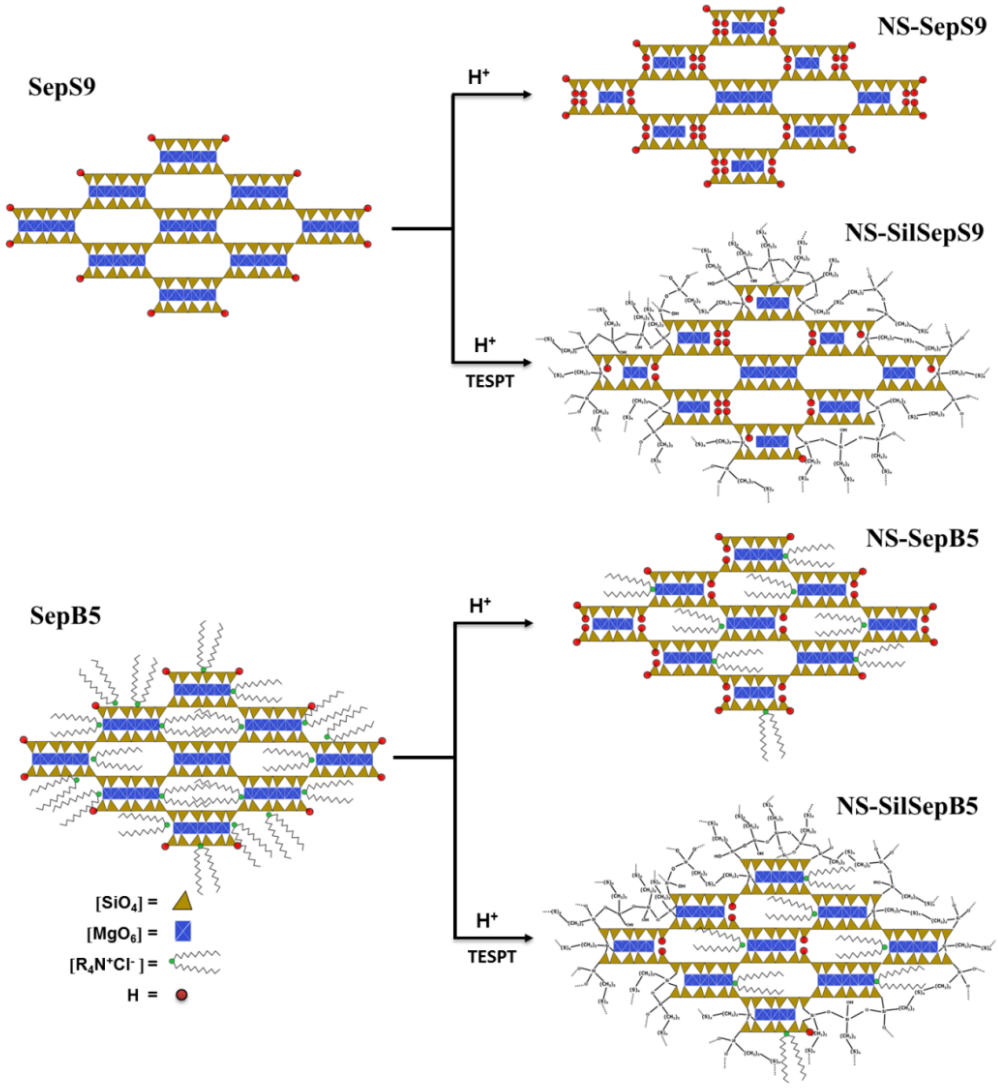

Scheme 1. Experimental procedure for acid treatment and for one-pot procedure of (a) SepS9 and (b) SepB5. The SepX structural representation consists of two tetrahedral silica sheets and a central octahedral Mg sheet. In evidence, the partial extraction of structural Mg^{2+} from the octahedral sheet, the increase of silanol groups on the sepiolite surface and the TESPT silanization on the sepiolite surface.

2.3. One-pot procedure for acid treatment/silanization SepS9 and SepB5

Functionalized Sep fibers, labeled NS-SilSepX, were prepared simultaneously to the acid treatment by using TESPT as silane coupling agent (synthetic pathway with H^+/TESPT in Scheme 1). TESPT (64.7 g) was added

to the HCl mixture containing SepX (120.0 g). The reaction conditions and workup procedure were the same as those reported above (Paragraph 2.2).

2.4. Preparation of Sep/SBR nanocomposites

Uncured composite materials were prepared by blending technique in a Brabender Plasti-Corder lab station internal mixer (65 mL mixing chamber, 0.6 filling factor) for filler incorporation in SBR matrix. This technique is well-known in the rubber industry and described in various ASTM standards for the preparation of rubber composites (ASTM D 3188, D 3185 1A). The whole procedure consisted of three mixing steps performed at different temperatures (140, 90 and 50 °C), according to the thermal stability of the reactants. In the first step, rubber was masticated at 140 °C and 60 rpm rotor speed; then pristine or modified Sep clays (35 phr) were added in three subsequent aliquots, together with TESPT (2.8 phr). Two minutes after the last filler addition, 6PPD (2 phr), zinc oxide (3.5 phr) and stearic acid (2 phr) were added; this lag time avoids secondary reaction between ZnO and silica silanols. In the second step, the obtained materials were reloaded in the internal mixer operating at 90 °C at 60 rpm. CBS (3 phr) and sulfur (1 phr) were then added and mixed for 2 min. In the last step, the composites were finally processed in a two-rolling mill at 50 °C for 3 min. to improve their homogeneity. Uncured composites are labeled SepX/SBR, NS-SepX/SBR and NS-SilSepX/SBR. The reference material was prepared by using Silica Zeosil 1165 instead of Sep and labeled SiO_2/SBR. Finally, cured composites containing 35 phr of SepX, NS-SepX and NS-SilSepX were obtained, by vulcanization performed in a hydraulic press at 170 °C and 100 bar for 20 min. The conditions for the curing of composites were optimized as described in Paragraph 2.7. Vulcanized samples are called respectively V-SepX/SBR, V-NS-SepX/SBR and V-NS-SilSepX/SBR in the following. Cured reference material is called V-SiO_2/SBR.

The NS-SepX were incorporated in BR/IR matrix together with conventional silica and carbon black in technical compositions (TC) for vulcanisable elastomeric materials. The mixing was conducted in three steps using an internal tangential rotor mixer : in the first step, BR/IR (60/40 phr), NS-SepX (7 phr), silica (10 phr), carbon black (35 phr) and TESPT (5 phr) were introduced and the mixing was continued for 5 min, heating up to 135 °C, when the composition was unloaded. After 12 h, in the second step, ZnO (4 phr), stearic acid (1 phr), TMQ (1 phr) and 6-PPD (1.5 phr) were added and mixed for 3 min, up to 125 °C, when the composition was

unloaded. After 12 h, in the third step, TBBS (4 phr) and sulphur (2.3 phr) were added and mixed for 2 min, up to 95 °C. These materials, namely V-NS-SepX/TC, were compared with the same elastomeric materials with only silica (20 phr), called V-SiO_2/TC. The compositions of the TC materials was summarized in Table S1 of the Supporting Information (SI).

2.5. Morphological, structural and spectroscopic characterization of Sep fibers

Morphology of Sep samples was investigated by Scanning Electron Microscopy (SEM) analysis, performed by a Vega TS5136 XM Tescan microscope (Fig. S1a,b and S2 of SI). The electron beam excitation was 30 kV at a beam current of 25 pA, and the working distance was 12 mm. In this configuration the beam spot was 38 nm sized. Prior to SEM analysis, samples were gold-sputtered.

Morphological characterization of SepX, NS-SepX and NS-SilSepX was performed on a Jeol 3010 High Resolution TEM (HR-TEM) operating at 300 kV with a high-resolution pole piece (0.17 nm point to point resolution) and equipped with a Gatan slow-scan 794 CCD camera. The powders were suspended in iPr-OH, and a 5 μL drop of this suspension was deposited on a holey carbon film supported on 3 mm copper grid for TEM investigation.

The crystal structure of Sep samples was investigated by X-Ray Diffraction (XRD), recorded in X'Pert Pro PXRD (Panalytical) diffractometer in Bragg-Brentano geometry, using Cu K-α source 1.54 Å length. The degree of functionalization of NS-SilSepX with TESPT was estimated by CHNS analysis and reported in Table S2 of SI.

The thermal degradation profile of Sep samples was obtained through thermogravimetric analysis (TGA) at constant N_2 flow (50 mL min^{-1}) and heating rate of 5 °C min^{-1} in the range 30-150 °C, and at constant air flow (50 mL min^{-1}) and heating rate of 10 °C min^{-1} in the range 150-1000 °C. TGA curves are reported in SI (Fig. S3 and S4).

The fraction of Mg^{2+} cations leached during the acid treatment was determined by Inductively Coupled Plasma Atomic Emission Spectrometry (ICP-AES), using a PerkinElmer OPTIMA7000 DV spectrophotometer. Acid treatments were carried out in a reaction flask under mechanical stirring as previously described in the

Paragraph 2.2. During the acid attack, samples of 5 mL were withdrawn at intervals of 10 min and separated by centrifugation. Thus the Mg^{2+} content of the supernatant was analyzed. ICP data are reported in Fig. S5 of SI.

Chemical surface modification of Sep was studied by Attenuated Total Reflection-Fourier Transform Infrared Spectroscopy (ATR-FTIR), performed on a Perkin Elmer Spectrum 100 instrument (1 cm^{-1} resolution spectra, 650-4000 cm^{-1} region, 16 scans). Vibrational frequencies are reported in Table S3 of SI.

Sep fillers were also characterized by solid-state Nuclear Magnetic Resonance (SS-NMR) with a Bruker 400WB spectrometer operating at a proton frequency of 400.13 MHz. Magic Angle Spinning (MAS) NMR spectra were acquired with cross polarization (CP) and single pulse (SP) sequences. CP experiments: ^{13}C frequency 100.48 MHz, π/2 pulse length 3.5 μs, contact time 2 ms, decoupling length 6.3 μs, recycle delay 5 s, 2k scans. SP sequence: ^{29}Si frequency 79.48 MHz, π/4 pulse 3.9 μs, recycle delay 100 s, 1k scans; ^{1}H frequency 400.13 MHz, π/2 pulse length 5 μs, 16 scans. Samples were packed in 4 mm zirconia rotors, which were spun at 9 kHz under air flow. Adamantane, Q_8M_8 and EtOH were used as external secondary references. Si units are labeled according to the usual NMR notation: T^n and Q^n represent trifunctional $CSiO_3$ and tetrafunctional SiO_4 units, respectively and n is the number of oxo-bridges. ^{29}Si NMR chemical shifts are reported in Table S4 of SI. ^{13}C CPMAS and ^{1}H MAS NMR spectra are reported in Fig. S6 and S7 of SI.

2.6 Morphological characterization of uncured and cured Sep/SBR nanocomposites

The morphological investigation of both uncured and vulcanized composites was carried out by TEM using a Zeiss EM 900 microscope. Ultrathin sections (about 50 nm thick) of composites were obtained with a Leica EM FCS cryo-ultramicrotome, equipped with a diamond knife, by keeping the samples at -130 °C.

ImageJ processing program (Image Processing and Analysis in Java) was utilized to measure manually the of Sep fibers embedded in the elastomer matrix. An example of ensuing normalized histograms is documented in Fig. S8 of SI.

2.7 Dynamic-mechanical analysis of cured and uncured Sep/SBR composites

Curing profiles of uncured composites were measured with Rubber Process Analyzer (RPA2000, Alpha Technologies) under the following conditions: ±1° oscillation angle, 170 °C temperature, 15.65 kPa pressure

and 30 min running time. This analysis gave the optimal conditions for the curing of composites (see Paragraph 2.4).

The Sep percolation threshold was estimated on the basis of the Hüber-Vilgis plot (Hüber and Vilgis 1999). The percolation threshold was 30 phr on average. Based on this result, the composites were prepared with 35 phr of Sep (that is above the percolation threshold) in order to favor the formation of a network of interacting particles, diffused through the whole matrix (Figure S9 of SI).

Dynamic-mechanical measurements on nanocomposites were performed with the same rheometer operating in the shear stress mode. For the uncured samples the strain sweep tests were carried out at 70 °C and 1 Hz from 2 to 100 % of elongation. In the case of cured samples the strain sweep was carried out at 70 °C and 10 Hz.

Specimens for RPA analysis were cut by using a Constant Volume Rubber Sample Cutter (CUTTER 2000, Alpha Technologies); the dimensions were 3.5 cm diameter and ≈ 0.2 cm thickness, the weight 4.5 ± 0.3 g. Two measurements were carried out for each sample, and the average value was reported.

3. Results And Discussion

3.1 NS-SepX and NS-SilSepX

According to the literature (Yebra et al., 2003), the acid treatment of Sep generally leads to partial or total destruction of the magnesium octahedral sheets in the structure with the formation of amorphous silica. Instead, the treatment here described aims at: i) favoring the magnesium extraction but preserving the Sep structure and morphology, and ii) increasing the number of reactive silanol groups on the Sep surface, improving the clay interfacial reactivity. The simultaneous functionalization with TESPT allows to obtain *ex-situ* modified Sep fibers suitable for compatibilization with rubber composites. Two different kinds of commercial Sep clays, namely the standard SepS9 and the organically modified SepB5, were chosen.

The morphology of the pristine SepX and modified NS-SepX and NS-SilSepX samples was investigated by SEM and TEM analyses (Fig. S1, S2). SepS9 and SepB5 present fibers strongly interconnected in bundles-like aggregates, in agreement with the literature (Alvarez, 1984). The fiber size is practically the same for both

SepS9 and SepB5, while the way, through fibers gather together to form bigger fibrous structures. slightly varies.

After acid treatment, NS-SepX samples (Fig S2) exhibit significant disaggregation and the fibers show parallel orientation without tangles, as in SepX. In addition, the treatment produces a remarkable decrease of the fibers length (see dimensional data from TEM analysis reported in Table).

The acid treatment in the presence of TESPT gives rise to similar changes (Fig. 1). HR-TEM images reveal a uniform silane coating of the fiber surface, clearly distinguishable from the silicate fiber (insets of Fig. 1).

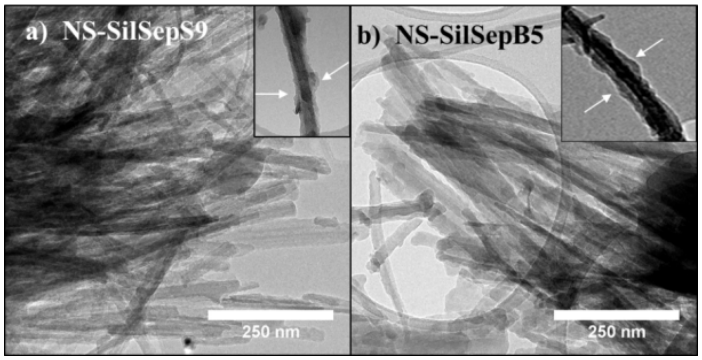

Figure 1. TEM images of (a) NS-SilSepS9 and (b) NS-SilSepB5. In the insets, the HR-TEM of an individual fiber of NS-SilSepX.

On the basis of CHNS data (Table S2 of SI), the degree of functionalization of NS-SilSepX with TESPT was estimated about 18 wt.% for both NS-SilSepS9 and for NS-SilSepB5. This suggests that most of TESPT reacts with the Sep surface, as further confirmed by NMR investigation (see later). The occasional presence of few spherical nanoparticles was associated to a possible silane self-condensation reaction as reported in similar procedures (Garcia et al., 2011).

XRD analysis confirmed that the acid treatment and the functionalization process do not alter the Sep crystalline structure (Fig. 2). In fact, the diffractograms of pristine SepX (Yebra et al., 2003) are strictly comparable to those of the materials obtained after 2h of HCl contact. Only small changes in relative intensity and width of the reflections of Sep samples were observed. In particular, based on the Scherrer equation, the slight broadening

and weakening of (110) reflection of the modified Sep suggests that acid treatment produces a decrease of size of Sep fibers.

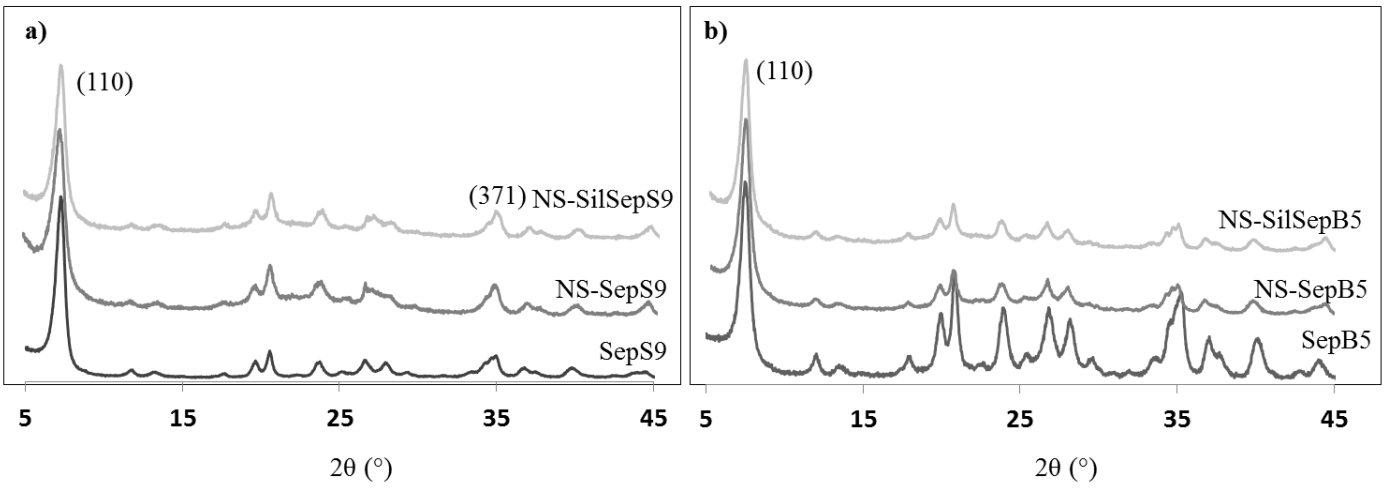

Figure 2. XRD patterns of (a) SepS9 (black), NS-SepS9 (grey), NS-SilSepS9 (light grey) and (b) SepB5(black), NS-SepB5 (grey), NS-SilSepB5 (light grey).

The changes in Sep chemical structure were studied by ATR-FTIR. The spectra of pristine and modified Sep samples are shown in Fig. 3. In addition, the characteristics vibrations are listed in Table S3. The NS-SepS9 spectrum (black line in Fig. 3a) evidences the adsorption bands at 3700-3555 cm^{-1}, attributable to the stretching vibrations of OH groups and water molecules bounded to octahedral magnesium centers, and at 692 cm^{-1}, assignable to the Mg-O-H bending vibrations (Cornejo and Hermosin, 1988). Although reduced in intensity with respect to pristine Sep (black dashed line in Fig. 5a), these peaks confirm that the Mg–OH bonds were only partially destroyed by the acid treatment.

Simultaneously, the band at 3754 cm^{-1}, assigned to structural hydroxyls belonging to silanol groups, increases in intensity mainly in NS-SepS9 indicating the formation of the reactive silanol groups after acid treatment. In fact, the bands at 1057 and 1018 cm^{-1} belonging to the Si–O units of tetrahedral merge into one peak occurring at 1068 cm^{-1}, which is associated to amorphous silica (Moenke 1974). Moreover, the band of amorphous silica near 795 cm^{-1} increases in intensity along the acid treatment (Vincent et al., 1996; Komadel, 1999). The

changes of the Si–O stretching band and its shift toward 1068 cm^{-1} indicate a progressive release of the Mg atoms from the octahedral sheets. The NS-SilSepS9 spectrum (grey line in Fig. 3a) confirms the silane functionalization with the appearance of bands ascribable to the CH_3 and CH_2 stretchings (2977-2890 cm^{-1}) and the corresponding bending modes (1346, 1303, 1438 cm^{-1}) of TESPT.

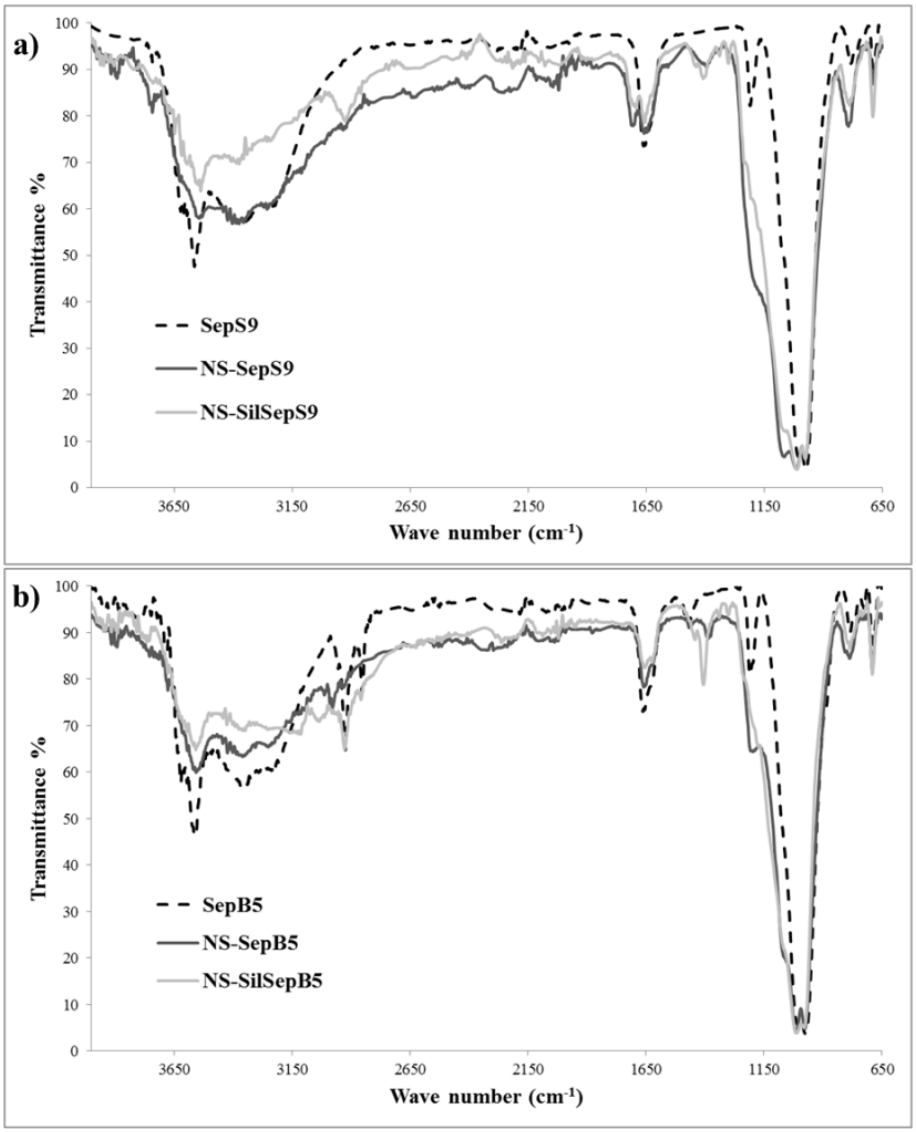

Figure 3. FTIR adsorption spectra of (a) SepS9 (black dashed line), NS-SepS9 (black line), NS-SilSepS9 (grey line) and (b) SepB5 (black dashed curve), NS-Sep B5 (black line), NS-SilSep B5 (grey line).

The SepB5 spectrum (black dashed line in Fig 3b) presents the vibrations of benzyl alkyl chain at 2923, 2849, 1661 cm^{-1}, in addition to the SepS9 absorption bands. NS-SepB5 (black line) and NS-SilSepB5 (grey line) spectra have similar trends and changes comparable to those described above for the SepS9.

In order to confirm the Sep structural changes due both to acid treatment and silanization reaction, the samples were also studied by multinuclear SS-NMR. Fig. 4 presents the comparison among the ^{29}Si MAS NMR spectra recorded on Sep based samples. The Si local environment is almost identical in SepX, pointing out that the organic modification in SepB5 does not affect the Si sites. The pristine SepX clays show four different Si sites, three Q^3 units accounting in the spectra for the well-resolved resonances with similar intensities, and the Q^2 unit represented by a small signal at about -85 ppm (Weir et al., 2002; D'espinose De La Caillerie et al., 1994). Each of the three main resonances has been attributed to one of the three pairs of equivalent Si nuclei in the basal plane, and the resonance at about -85 ppm to Q^2(Si-OH) Si nuclei (Weir et al., 2002) through COSY and HETCOR experiments: the resonance at -92.7 ppm was unambiguously assigned to the intermediate, near-edge Si sites (Si2); furthermore, the resonance at -94.3 ppm is assigned to the central Si position (Si3) since it cross-polarizes almost entirely with the Mg-OH protons; finally, the resonance at -98.2 ppm (Si1) is assigned to the edge Si sites because it strongly correlates to the protons of the structural water molecules (Weir et al., 2002). The SepX acid treatment causes in the spectra of NS-SepX: i) the disappearance of Q^2(Si-OH) peak, ii) the appearance of the broad resonances at about -100 and -110 ppm, due to Q^3 and Q^4 units in the amorphous SiO_2 and iii) the small shift of the resonances assigned to Si2 and Si3 in the basal plane. According to the literature (Aramandia et al., 1997), the Q^4 units derive from the partial dissolution of Mg^{2+} cations of the octahedral sheet (Yebra et al., 2003; Dékány et al., 1999) that leads to the formation of new silanol groups, in agreement with the presence of the Q^3 units.

The silanization treatment leads, in the spectra of NS-SilSepX, to the appearance of the signals at -56 and -65 ppm, respectively due to the T^2 and T^3 units derived from TESPT. The control experiments (data not shown) confirmed that the reaction of Sep with TESPT in iPr-OH does not proceed in the absence of the acid treatment, since no peaks attributable to pristine or condensed TESPT were detectable in the corresponding ^{29}Si NMR spectra.

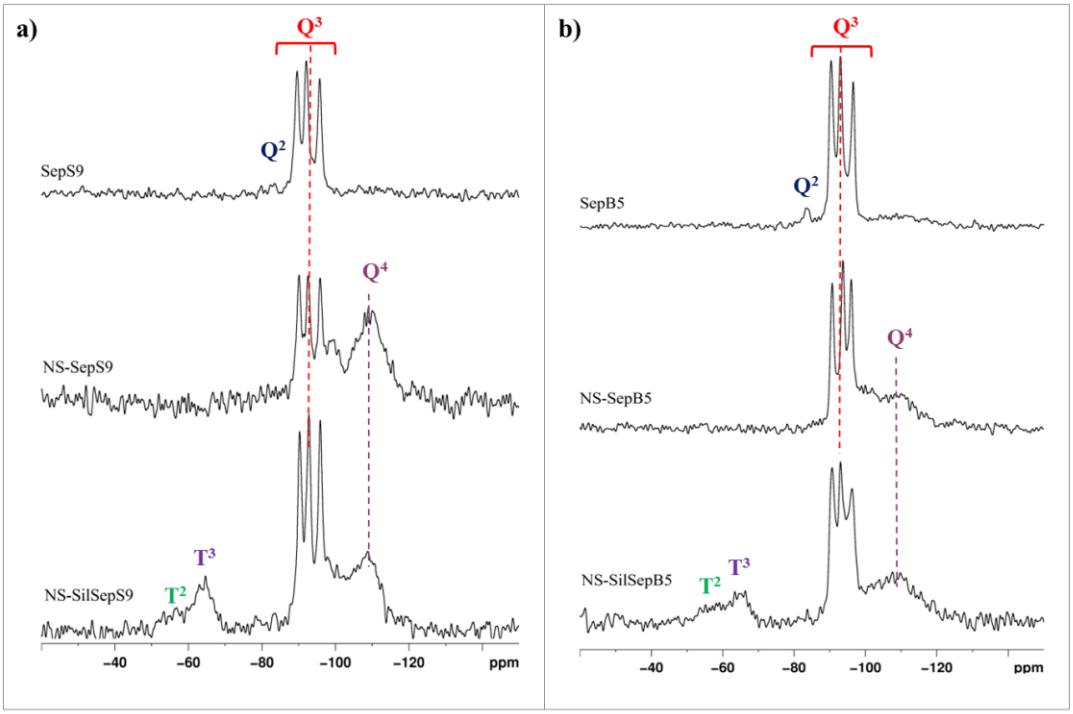

Figure 4. ^{29}Si MAS NMR spectra of (a) SepS9, NS-SepS9 and NS-SilSepS9 and (b) SepB5, NS-SepB5 and NS-SilSepB5.

The degree of TESPT condensation (DOC%) is about 90% and the Sep/TESPT ratio is about 100:20 in sample NS-SilSepS9. According to the results reported in Table S4, both DOC% and amount of TESPT are slightly lower in the samples prepared with SepB5. Interestingly, the position and the ratio among the three sharp Q^3 resonances of the clay are kept in both samples, thus demonstrating that the removal of Mg^{2+} cations and the silanization step takes place without depleting the original clay structure. The broad resonance due to Q^4 and Q^3 units in the amorphous silica accounts for about 56% and 46% of the whole Sep Si units, for NS-SilSepS9 and NS-SilSepB5 respectively. According to the results of Table S4, in the case of SepB5, the organic functionalization of Sep reduces the extent of the reactions both with the acid solution and the silane. The amount of amorphous silica decreases in both cases with TESPT addition with respect to the pure acid treatment.

The ^{13}C CPMAS spectra (Fig. S6) clearly show the differences between the two used SepX. Peak assignments are summarized in Table 1. As expected, the ^{13}C spectrum of SepS9 is featureless, since the pristine Sep does

not possess any organic component and no iPr-OH molecules are retained in the channels after acid treatment. Analogously, the spectrum of NS-SepS9 appears flat.

Table 1. ^{13}C NMR chemical shifts and assignments for SepB5 and SepS9 samples.

δ (ppm)	**Functional group**	
13.4	Si-CH_2-	TESPT
23.9	-CH_2-	TESPT
25.2	-CH_3	iPr-OH
32.9	-CH_2-	dodecyl chain, DMMA
41.7	-CH_2-S	TESPT
67.6	-CH_2-OH	iPrOH, (CH_2)-N^+ DDMA

On the contrary, SepB5 spectrum shows at about 33 ppm the signal of the methylene groups ascribable to the Sep functionalization with *N,N*-didodecyl-*N*-methylammonium; in addition, the sharp resonances of the iPr-OH trapped in the channels are clearly visible in the NS-SepB5 spectrum. In the spectra of both NS-SilSepX, the successful functionalization with TESPT is proved by the presence of the characteristic carbon signals of the propyl chain linked to the silicon atom. The presence of iPrOH is confirmed by the small broad peak at 67 ppm but no signals due to the –OEt groups are detected suggesting their complete hydrolysis in the presence of acid. It is worth of noting that NS-SilSepB5 spectrum shows again the partial presence DMMA siganls. The presence in SepB5 of organic molecules with large steric demand and locally affecting the medium polarity could be the reason for the lower yield in amorphous silica formation and TESPT functionalization with respect to SepS9, as pointed out by the ^{29}Si NMR study.

The ^{1}H MAS NMR spectrum of SepS9 (Fig. S7) presents two overlapped resonances. According to the literature (Komadel, 1993), the sharp component centred at -1.8 ppm is assigned to MgOH groups and the broad signal centred at 2.2 ppm is produced by the contribution of water molecules on the external surface of the Sep, both free to move inside the Sep tunnels and coordinated to magnesium. The acid treatment in iPr-OH (NS-SepSX) leads to the appearance of a new resonance at -0.9 ppm similar in intensity to that of MgOH signal. This peak is present in both the modified samples as the resonance at around 0.3 ppm. A very broad and intense peak at about 2 ppm is also present, broader in NS-SilSepS9, probably as a consequence of the overlapping with

the TESPT methylene signals. Aramendìa (Aramendìa et al., 1997) proposed that the formation of amorphous silica by Sep acid treatment leads to the appearance of new silanols. Therefore, in agreement with the signals of Q^3 units detected in the ^{29}Si spectra, the Si-OH functions could contribute to the proton spectrum with a signal around 2 ppm that overlaps to the water signal at 2.2 ppm. The ^{1}H spectra of SepB5 present some differences respect to those of SepS9, as a consequence of the organic modification and the favorable interaction with iPr-OH pointed out by the ^{13}C NMR spectra. In detail, the water resonance at 2.2 ppm peak is sharp according to the main contribution of the free water molecules entrapped in the tunnels with a low amount of external water (left shoulder). The MgOH peak is overlapped with other two intense sharp peaks at -0.8 and -1-1 ppm, probably due to the methylene protons of the dodecyl chain. The spectrum of sample NS-SepB5 shows the presence of peaks related to iPr-OH entrapment in the Sep channels, as already suggested by ^{13}C spectrum. The broadening increases after silanization due to the overlapping with the TESPT methylene signals, but the water resonance in NS-SilSepB5 appeared reduced in comparison to the corresponding signal in NS-SilSepS9.

In conclusion, the NMR results confirm that the acid treatment causes the formation of the amorphous silica by Mg extraction and, in these conditions, TESPT can hydrolyze and condense interacting with Sep, as clearly demonstrated by the TEM images. The SepB5 behavior appears conditioned by the organic modifier, which partially reduces the reactivity of the Sep against acid etching and silanization in comparison to SepS9.

ICP-AES analysis was performed to quantify the amount of extracted magnesium (Fig. S5) in relation with the presence of both TESPT and organic modifier of SepB5. The results are in perfect agreement with the NMR conclusions. The maximum fraction of Mg^{2+} leached after 2h of acid treatment was 80% for SepS9 and only 45% for SepB5, suggesting a lower extraction in the presence of DMMA. Besides, in the presence of TESPT, the percentage is lower with respect to the simple acid treatment (46% for SepS9 e 32% for SepB5). This suggests that the Mg^{2+}extraction is strongly affected by both TESPT and the organic modifier. In particular, we can hypothesize that, in the presence of TESPT, the Mg^{2+} extraction is accompanied by the linkage of organosiloxyl groups that form a layer coverage of the residual silicate. This coating should delay further extraction of Mg^{2+} ions. In the case of SepB5, the alkylammonium in the interlayers prevents the income of the

protons into the Sep interlamellar region, especially in the presence of TESPT (45% respect to 32% of extracted Mg^{2+}), as reported in the literature for different kind of clays (Breen et al., 1997).

This exhaustive analysis supports that the acid surface activation, here described, provides NS-SepX with reduced particle size, preserving the anisotropic features and increasing the bonding sites at the Sep surface.

3.2 NS-SepX/SBR and NS-SilSepX /SBR composites: curing, dynamic and mechanical behavior

Rheological and dynamic-mechanical analyses were performed in order to evaluate the effect of modified Sep fillers in comparison to bare Sep.

The rheometric characteristics of the Sep/SBR nanocomposites, expressed in terms of the minimum torque (M_L) and the maximum torque (M_H) are reported in Table 2.

Table 2. Curing Characteristic of Sep/SBR Nanocomposites.

samples	Scorch time (min)	M_L (Nm)	M_H (Nm)	M_H-M_L (Nm)
SepS9/SBR	2.67	2.73	13.36	10.63
NS-SepS9/SBR	4.08	2.47	10.43	7.96
NS-SilSepS9/SBR	4.35	2.38	14.65	12.27
SepB5/SBR	2.81	1.29	15.43	14.14
NS-SepB5/SBR	4.10	2.30	12.87	10.57
NS-SilSepB5/SBR	3.37	2.61	17.56	14.95

The minimum torque (M_L) (i.e., the torque at the initial stage of vulcanization), related to the viscosity of the compounds, is practically independent from the Sep used, reflecting a similar clay dispersion in the uncured samples. Only the SepB5/SBR composite showed lower M_L, likely due to the presence of some free ammonium salt in SepB5, acting as lubricant and secondary accelerator. The incorporation of the treated Sep fillers in SBR matrix gives satisfactory value of the maximum torque (M_H), which is a measure of crosslink density and stiffness of the rubber. In particular the enhanced M_H of NS-SilSepX/SBR with respect to both SepX and NS-SepX/SBR suggests excellent interaction between clay and rubber in modified NS-SilSepX cured composites, due to the presence of TESPT compatibilizer. Nanocomposite containing NS-SilSepB5 with better dispersibility

and surface chemistry shows the best interaction with the sulfur-based vulcanization compounds, leading to enhanced mechanical properties in the rubber composition. Probably, the presence of quaternary ammonium salts favour a quicker and more efficient curing of sulfur-based rubber compositions (Hakim and Ismail, 2008).

After evaluating the effectiveness of curing process, a detailed investigation of the dynamic-mechanical behavior of the composites was performed by RPA analysis, which allows to evaluate the effect of filler-filler interaction in the Sep network and of Sep-polymer interaction.. The storage modulus (*G'*) of the uncured and cured composites containing NS-SepX and NS-SilSepX, has been measured and compared with that of the composites containing pristine Sep (Fig. 5 and 6). A pronounced nonlinear dependence of modulus, known as Payne effect (Payne 1962), is observed in all cases. In fact, the G' value at low strain decreases rapidly by increasing the strain amplitude and, at large strain, it approaches the lowest value. This pronounced dependence of the modulus, referred to as Payne effect (Payne 1962), is associated to: (i) the presence of a filler network; (ii) the adsorption-desorption of polymeric chains at the filler interface; (iii) the disentanglement of bulk polymer from the rubber bounded to the filler surface; (iv) the strain-softening of the more rigid polymer shell surrounding the particles surfaces (Heinrich and Kluppel, 2002).

In details, before curing (Fig. 5a), the NS-SepS9/SBR and NS-SilSepS9/SBR samples show highest moduli at low strain (G'_0). At the highest deformation, the modulus (G'_∞) resulted very similar for all the composites

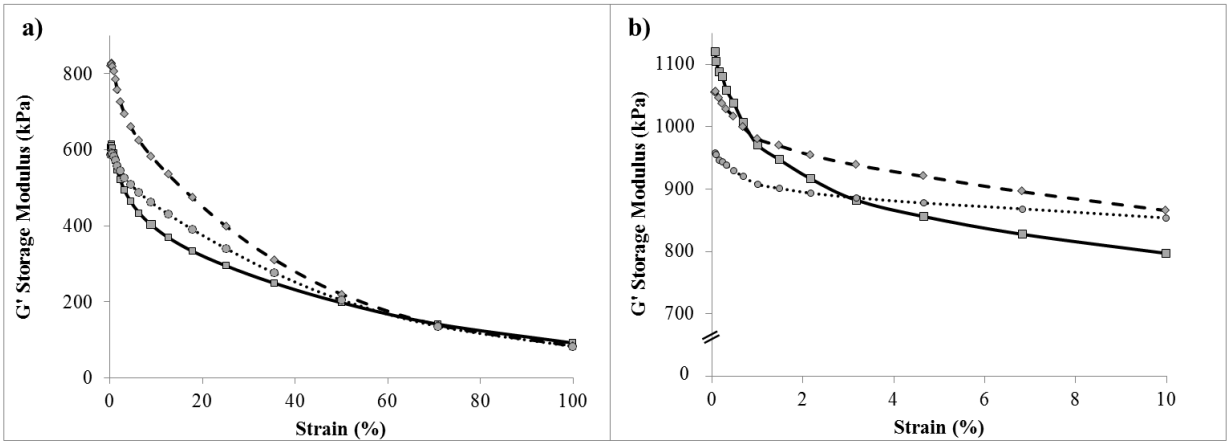

Figure 5. Storage modulus G' *vs* strain of (a) SepS9/SBR (black line), NS-SepS9/SBR (dashed line), NS-SilSepS9/SBR (dotted line) and (b) V-SepS9/SBR (black line), V-NS-SepS9/SBR (dashed line), V-NS-SilSepS9/SBR (dotted line).

After curing (Fig. 5b), a remarkable increase of the modulus either at low or at high strain was observed for all the composites. In particular the highest G'_0 value was obtained for V-SepS9/SBR, compared with V-NS-SepS9/SBR and V-NS-SilSepS9/SBR composites. Instead at high strain, the effect was much more pronounced for the NS-SepS9/SBR and NS-SilSepS9/SBR samples, resulting in the highest G'_∞ value. In any case, the composites containing modified Sep fibers display the lowest decrease of modulus versus strain, that is, the lowest Payne effect. This suggests a strong immobilization of the polymer chains close to the nanofibers surfaces or within their network, which increases the mechanical reinforcement of the composites. Evidently after acid treatment and *ex-situ* silanization, the interaction of fibers with the polymer chains improves as well as the cross-linking coupling because of the higher number of bonding sites.

Fig. 6 shows the RPA analysis of SepB5 composites. The storage modulus of SepB5/SBR, NS-SepB5/SBR and NS-SilSepB5/SBR (Fig. 6a) presents trends similar to those of the corresponding SepS9 composites. In comparison to the SepS9/SBR (line black in Fig. 5a), G'_0 value of SepB5/SBR is approximatively 50% lower, corresponding to 300 KPa. This suggests the presence in SepB5 of some free quaternary ammonium salt, which is a powerful lubricant and thus is able to reduce viscosity and modulus of uncured rubber, in agreement to the M_L value of Table 3. After curing, the data in Fig 6b show: i) increase of the modulus both at low and high strain; ii) higher G'_0 value of V-SepB5/SBR; iii) higher G'_∞ value of V-NS-SepB5/SBR and V-NS-SilSepB5/SBR; iv) $\Delta(G'_\infty-G'_0)$ values much lower in V-NS-SepB5/SBR and V-NS-SilSepB5/SBR than in V-SepB5/SBR.

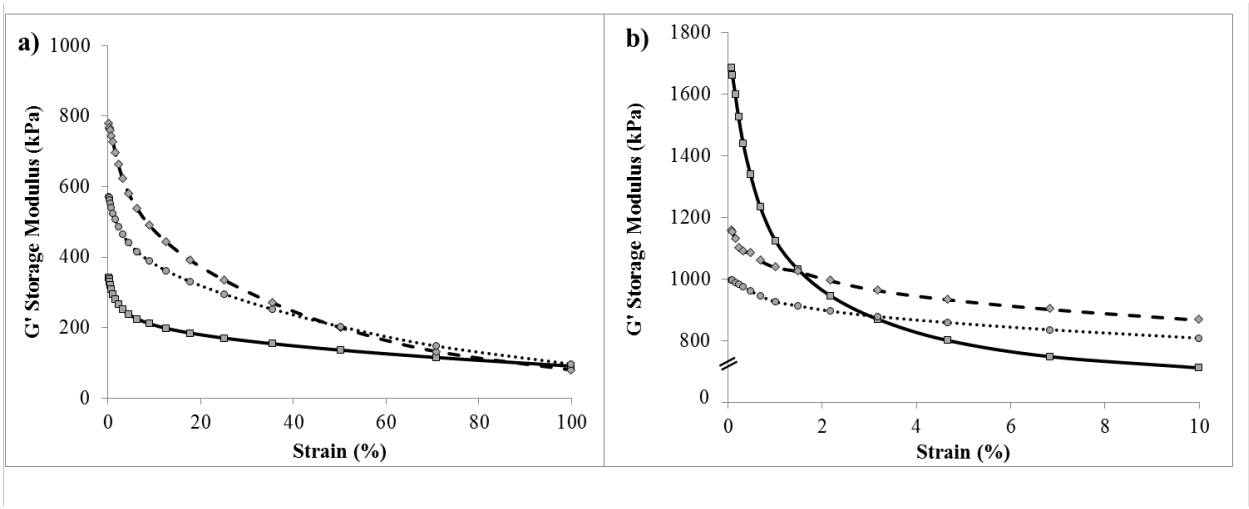

Figure 6. Storage modulus G' *vs* strain of (a) SepB5/SBR (black line), NS-SepB5/SBR (dashed line), NS-SilSepB5/SBR (dotted line) and (b) V-SepB5/SBR (black line), V-NS-SepB5/SBR (dashed line), V-NS-SilSepB5/SBR (dotted line).

As ammonium salts are known to enhance curing, their possible presence in V-SepB5/SBR, while explaining the high MH value recorded at 170°C, does not account for the dramatic Payne effect observed for this composite. Indeed, curing effects concern the polymer phase and are largely strain-independent. Thus, the large Payne effect of Sep (pristine or organically modified) in cured rubber compounds can be attributed to low filler-rubber interaction, which makes the filler network very sensitive to strain (Nahmias Nanni et al., 2012).

To better understand the variation in mechanical properties due to NS-Sep fibers with respect to SepX and to the standard nanosilica, we report the values of G'(9%), $\Delta(G'_{\infty}-G'_{0})$ and loss tangent as Tan Delta (9%), which represent respectively the measure of reinforcement, Payne effect and hysteresis in vulcanized rubbers (Table 3).

Table 3. Dynamic properties: Storage modulus (9%), Payne effect as G'(0.5)-G'(10), Loss factor as TanDelta (9%) of V-NS-SepX/SBR and V-NS-SilSepX/SBR composites in comparison to the standard V-SiO_2/SBR and V-SepX/SBR composites.

	G'(9%) (MPa)	**G'(0.5)-G'(10)** (MPa)	**TanDelta (9%)***
V-SiO_2/SBR	0.834	0.252	0.081

V-SepS9/SBR	0.797	0.242	0.084
V-NS-SepS9/SBR	0.866	0.152	0.105
V-NS-SilSepS9/SBR	0.854	0.077	0.052
V-SepB5/SBR	0.705	0.614	0.132
V-NS-SepB5/SBR	0.864	0.218	0.089
V-NS-SilSepB5/SBR	0.807	0.153	0.072

***Calculated as ratio of the G' and storage modulus (G") at 9 % of strain

Compared with SepX, both NS-SepX and NS-SilSepX produce an enhanced reinforcement, consisting in the higher G'(9%) value. Interestingly the G'(9%) value of all sepiolites based samples are in the same range of that of silica composite, while the Payne effect for both V-NS-SepX/SBR and V-NS-SilSepX/SBR turns out to be lower than those of the composites both featuring commercial silica (V-SiO_2/SBR) and enclosing untreated Sep samples (V-SepS9/SBR and V-SepB5/SBR).

Finally, the dynamic loss tangent of NS-SilSepX fibers in SBR matrix are significantly reduced, both with respect to commercial silica and to the untreated Sep. This result suggests that when Sep is functionalized *ex-situ* during the acid treatment procedure (as for V-NS-SilSepX) the compatibilization reaction is complete, resulting in a significant improvement of filler-rubber interaction. The tan δ values at 10 Hz and 9% of dynamic strain is a good indicator of rubber material hysteresis and can be associated to the rolling resistance. For this, from the results reported in Table 3, it appears that NS-SilSepX nanofibers significantly improve rolling resistance without having a negative effect on reinforcement.

The NS-SepS9 and NS-SepB5 fibers were also formulated in TC for vulcanisable elastomeric materials of internal tyre components, suitable for various applications, such as elastomeric under-layer materials (car and heavy vehicles), soft bead (heavy vehicles), sidewall insert (car), or sidewall. These materials, namely V-NS-SepS9/TC and V-NS-SepB5 /TC were compared with reference elastomeric materials, V-SiO_2/TC, comprising standard silica as filler. The TC elastomeric materials were subjected to measurement of the static and dynamic mechanical properties, resumed in Table 4.

Table 4. Dynamic-mechanical characterization of TC Sep nanocomposites.

	V-SiO_2/ TC	V-NS-SepS9/TC	V-NS-SepB5 /TC
Traction			
E' 50%[a] [MPa]	1.99	2.51	2.47
E' 100%[a] [MPa]	4.05	5.44	5.42
Tensile strength [MPa]	12.33	12.27	12.58
Elongation at break (%)	255.0	199.70	191.99
Hardness			
IRHD[b] 23 °C	72.8	72.4	72.4
IRHD 100 °C	71.6	71.7	71.7
Dynamic compression			
E' [MPa][a] 23 °C 100 Hz	9.22	8.55	8.65
70 °C 100 Hz	8.97	8.65	8.66
T. DELTA[d] 23 °C 100 Hz	0.104	0.075	0.074
70 °C 100 Hz	0.069	0.052	0.050

[a] E' 50% and E' 100% tensile modulus at 50% and 100% deformation, respectively; [b] IRHD International Rubber Hardness Degrees; [c] E' dynamic elastic modulus; [d] T. DELTA (loss factor) calculated as the ratio between in terms of dynamic elastic modulus (E').

As a formulation is here concerned, 7 phr of NS-SepX were substituted with 10 phr of silica in order to compare compounds with similar stiffness, measured as dynamic compression modulus E' at 70°C. The analysis of the data in Table 4 shows that the incorporating of both NS-SepS9 and NS-SepB5 in the elastomeric material, in replacement of an aliquot of silica, produced higher tensile modulus without affecting tensile strength. For both V-NS-SepX/TC composites, E' 100% increase of more than 20% with respect to reference at comparable value of tensile strength. This effect can be tentatively explained in terms of a strain induced fiber alignment that is known to affect nanocomposites stiffness under tensile strain (Okamoto et al., 2001). Above all, the dissipative properties, measured as Tan Delta in compressive test improve drastically. In fact, the tan delta at 70 °C is lower than 25% in the compression test in the case of NS-SepS9 and NS-SepB5, due to the improved hysteresis imparted by the modified fibers. This result is even more significant if we consider that the composition was modified by less than 6% by weight. The TC-samples with NS-SilSepS9 and NS-SilSepB5 (data not shown) confirmed the same dynamic-mechanical behavior.

In summary, from the dynamic-mechanical analyses performed on the nanocomposites, it is clear that the presence of NS-Sep fibers generated by the acid treatment, decreases the Payne effect and hysteresis of the elastomeric materials while maintaining a good reinforcement.

3.3 Morphology of V-NS-SepX/SBR and V-NS-SilSepX/SBR composites

The effect of the acid treatment on the size and the dispersion of Sep fibers was investigated by TEM analysis of crude and cured composites. Thus morphological observations were correlated to the dynamic-mechanical data in order to highlight the role of the Sep nanofibers in enhancing the functional properties.

TEM images of V-SepS9/SBR, V-NS-SepS9/SBR and V-NS-SilSepS9/SBR are reported in Fig. 7 (images of corresponding uncured composite are reported in Fig. S10). Images at low magnification (Fig. 7 a,b,c and Fig. S10 a,b,c) testify the particle distribution in relatively large areas of the composites. In all samples, the composite materials exhibit a partial aggregation of Sep fibers. Especially in the V-NS-SepS9/SBR and V-NS-SilSepS9/SBR, the rubber matrix shows several zones poorer in filler particles. That is, the polymer network appears to be more discontinuous in samples containing modified Sep fibers than in samples with pristine SepS9. However, images at higher magnification (Fig. 7 a', b', c' and Fig. S10 a', b', c') reveal a more complex spatial distribution of fibers. In the Fig. 7a', V-SepS9/SBR shows exclusively individual fibers and tactoids, homogenously distributed in the matrix without any preferential orientation. The individual fibers preserve the geometric size of pristine Sep and the anisotropic feature (Table 5), as from representative TEM images. The AR values for SepS9 is about 30, while the length and cross-section are 770±187 and 24±7 nm respectively. Instead, in the V-NS-SepS9/SBR and V-NS-SilSepS9/SBR composites, the fiber size, due to acid treatment, are reduced: AR is 4 for NS-SepS9 and 23 for NS-SilSepS9. Interestingly, when the fibers length decreases, a preferential self-organization of the particles in anisotropic structures occurs. TEM images clearly show the presence of "filler network structures", consisting not only of directly interacting particles, but also of polymer chains bridging the particles. This filler-rubber interaction is evident by rubber layer surrounding the particles (see the insets in Fig. 7 b', c').

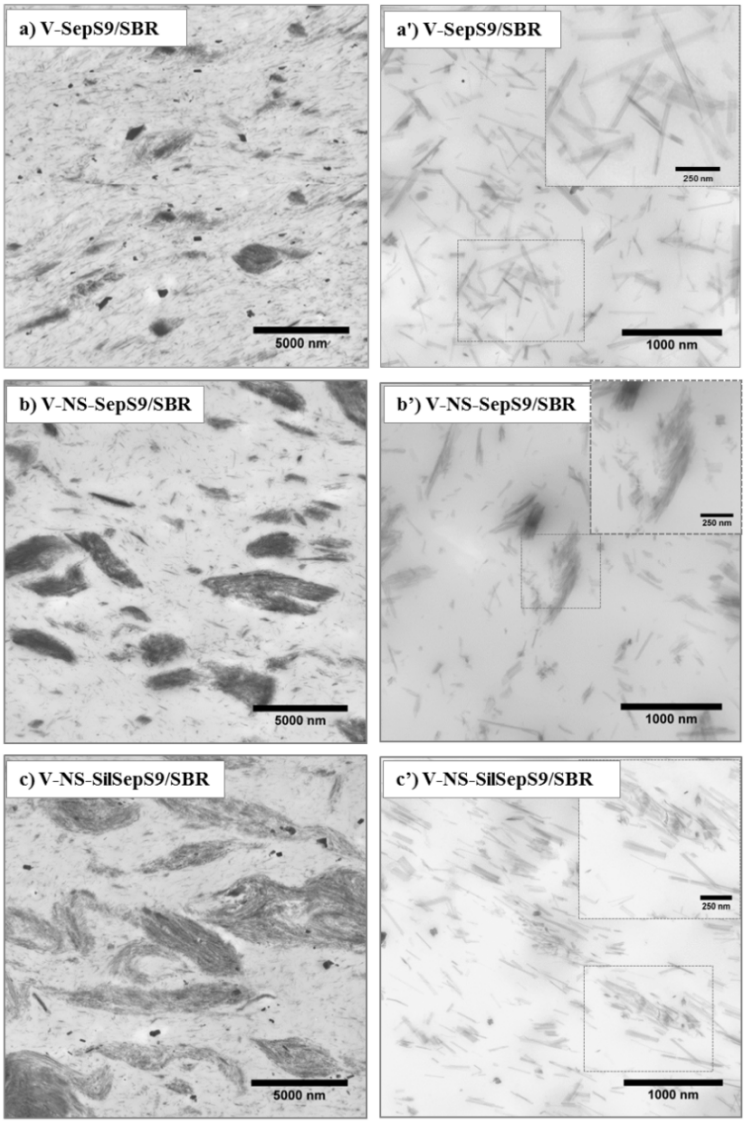

Figure 7. TEM images at different magnifications of (a, a') V-SepS9/SBR, (b, b') V-NS-SepS9/SBR, (c, c') V-NS-SilSepS9/SBR.

The wideness of *network structures* ranges from 0.57 to 0.87 micron in V-NS-SepS9/SBR, while in V-NS-SilSepS9/SBR it is about 0.27-1.3 μm. Particle alignment is diffused in the whole rubber matrix and the filler network structures seem not oriented in a *preferential* direction. This fiber organization occurs in spite of the mixing process used to obtain the composites and though no external or internal procedure was performed to drive the particle arrangement (Vaia and Maguire, 2007). This filler networking phenomenon is in agreement with a non linear dependence of G' on the strain amplitude (Fig. 5).

Table 5. Size dimensions* of SepX, NS-SepX and NS-SilSepX and corresponding filler network structure, obtained by TEM analysis.

	INDIVIDUAL FIBER			FILLER NETWORK STRUCTURE	
	Length (nm)	**Cross-section** (nm)	**AR**	**Length** (nm)	**Cross-section** (nm)
SepS9	767±187	24±7	**30 ± 16**	–	–
NS-SepS9	88±29	21±6	**4 ± 2**	1488±468	567±213
NS-SilSepS9	484±157	20±6	**23 ± 14**	1076±286	275±85
SepB5	886 ± 244	20.3±6.2	**44 ± 25**	–	–
NS-SepB5	348 ± 93	29±12	**12 ± 8**	988±400	526±73
NS-SilSepB5	523 ± 198	33±19	**15 ± 14**	1497±308	410±79

*Calculated as average of 29 fibers in 3 different TEM micrographs

Fig. 8 shows TEM images of V-SepB5/SBR, V-NS-SepB5/SBR and V-NS-SilSepB5/SBR composites (images of corresponding uncured composites are reported in Fig. S11 of the SI).

By images at low magnification of SepB5 samples (Fig. 8 a, and S11 a), it is evident that the quaternary ammonium salt improves the compatibility between fibers and SBR matrix, and thus the SepB5 dispersion (compare Fig. 8a and 9a), also thanks to the repulsion of the charges present on the SepB5 particles. In addition, the SepB5 fibers are totally oriented in V-SepB5/SBR sample (Fig. 8 a and a'), while they are randomly dispersed in SepB5/SBR (Fig. S11 a and a'). As well documented in the literature (Hobbie, 2010), this orientation occurs when anisotropic particles were subjected to shear strain of the RPA analysis during vulcanization process. This phenomenon does not appreciably occur for SepS9 because of strong inter-particle aggregation (Figures 7 a and a'). After acid treatment, TEM analysis again display a complex structural distribution of the modified NS-SepB5 and NS-SilSepB5 (Fig. 8 b, c and Fig. S11 b, c). Once more, fibers spontaneously assemble and form filler network structures, approximately of cross-section about 530 nm for

NS-SepB5 and 410 nm for NS-SilSepB5. Also in this case, the reduced size dimensions of individual Sep fibers (Table 5) can be related to the typical networking distribution in the ensuing NS-SepB5 and NS-SilSepB5 composites.

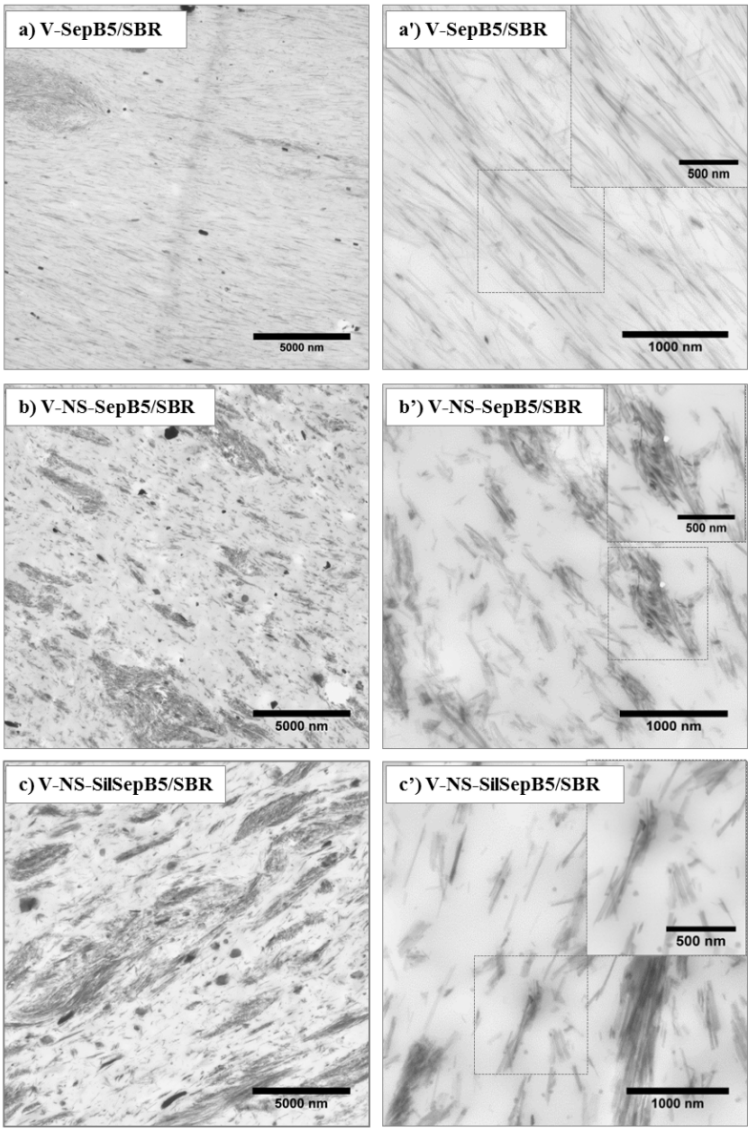

Figure 8. TEM images at different magnifications of (a, a') V-SepB5/SBR, (b, b') V-NS-SepB5/SBR, (c, c') V-NS-SilSepB5/SBR.

It's interesting to note that the surface modification and the decrease in particle size obtained by the acid treatment are triggering the filler network self-assembly. Self-assembly of particles is as an important process where the building blocks spontaneously organize into ordered structures and it is promoted by different

constraints (Grzelczak et al., 2010). In rubber-like materials, the filler self-assembly depends on the competition and delicate balance between two opposite actions: on one hand the hydrophilic particle cores tend to contact each other to shield themselves from organic matrix, on the other hand they interact with polymeric chains thanks to the presence of silane functional groups (Akcora et al., 2009). The particle shape as well as their interaction with polymer chains determine the *ordered structures* in which they can assemble Moreover, also the size of the anisotropic particles are crucial, since they have to be small enough to physically align and accommodate within the hosting polymeric architecture (Mann, 2009). In this respect, TEM analysis of V-NS-SepX/SBR and V-NS-SilSepX/SBR strongly suggests that only the sepiolite fibers, which are interfacially activated and display reduced particle dimensions, succeed to align and yield strong specific interactions which permit to the polymer chains to efficiently diffuse into the interspace of the modified fibers. This disrupts the tactoids interaction and favors the filler network self-assembly, as shown in the Scheme 2.

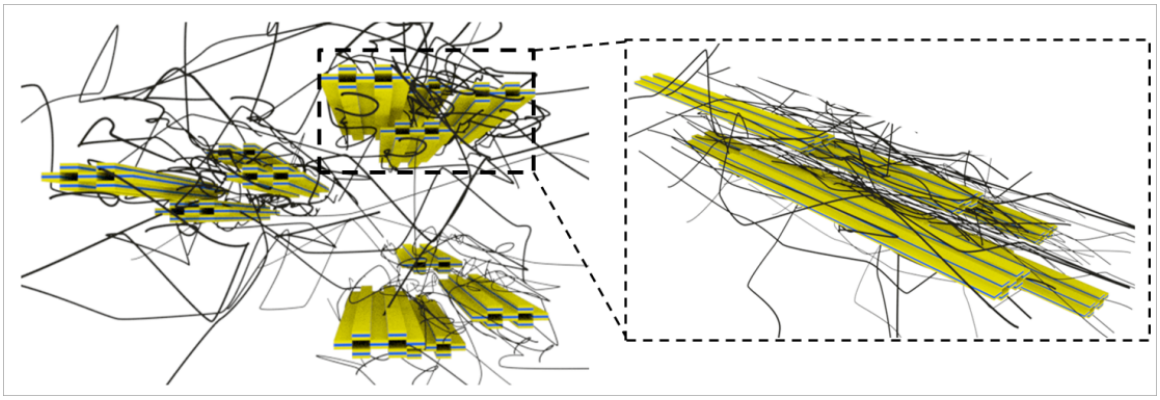

Scheme 2. Schematic representation of self-assembly of NS-SepX/SBR and NS-SilSepX/SBR.

The existence of the filler network self-assembly agrees with the reported mechanical performance. In fact, the pristine SepS9 and SepB5 do not show a significant reinforcement effect (with respect to nanosilica, in Table 3), as it would be expected on the basis of their high AR (Scotti et al., 2015). Moreover, despite the good distribution of the SepS9 and SepB5, as shown in the TEM images (a in Fig. 7 and 8), the filler-rubber interaction of corresponding composites is low even in presence of the TESPT compatibilizer. On the contrary, although the fibers distribution appears not homogeneous and discontinuous (b and c in Fig. 7 and 8), the NS-

SepX and NS-SilSepX produce a slightly higher value of reinforcement indicator (G'(9%)) and an improved hysteretic behavior in both SBR and TC nanocomposites. It is evident that the presence of network structures of sepiolite fiber (b' and c' in Fig. 7 and 8), connected by thin polymer films, is dominant in determining the performance of investigated composites. More in depth, the filler network structures are observed only in the presence of fibers with specific size and surface functionality, obtained by a controlled acid treatment and therefore able to self-assemble. While filler homogenous distribution is believed to critically affect mechanical properties, we here found that the self-assembly into highly anisotropic structures can optimize the macroscale properties, if such particle organization is repeated in a continuous manner throughout the whole polymer matrix. It could be suggested that the design of high performance materials requires excellent control over filler spatial distribution. Further quantitative experiments are currently in progress in order to better support these suggestions.

4. Conclusions

Nano-sized anisotropic NS-SepX fibers were obtained thanks to a controlled acid treatment, which allows to maintain the particle morphology while tuning the surface chemistry. NS-Sep fibers were used by *ex-situ* blending to prepare SBR nanocomposites whose mechanical properties were extensively evaluated and compared to those obtained by using pristine Sep as filler. The mechanical performance has been studied and related with the size and self-assembly of anisotropic Sep clays. NS-Sep fibers improve the reinforcing and hysteretic properties of rubber materials.

To summarize, we demonstrated that:

- The acid treatment increases the *number of silanol sites* on the Sep surface and reduces the *particle size* while preserving anisotropic features;
- The increased bonding sites on the Sep edge surfaces improve the *interfacial chemical interaction* between sepiolite fibers and rubber, increasing the fraction of the rigid polymer phase.

- Inside the elastomeric matrix, the *smaller size* allows the self-assembly of fibers in Sep network structures. This organization seem to be critical to improve the mechanical properties of both NS-SepX/SBR and NS-SilSepX/SBR with respect to the large-sized SepX and isotropic silica.
- Vulcanisable elastomeric materials containing modified Sep fibers show excellent properties of curing, reinforcement and hysteresis respect to conventional materials with standard silica filler.

These results suggest the use of anisotropic and nano-sized NS-SepX fibers as promising filler for energy saving tires (Giannini et al., 2015). In the state of the art there is no reference to use advantageously, as additional fillers in rubber and tire materials, needle-like Sep nanofibers.

In conclusion, our approach is a simple and effective method to prepare Sep nanocomposites suitable for advanced technological applications.

Acknowledgments

This work was in the frame of the European COST action MP1202 "Rational design of hybrid organic-inorganic interfaces: the next step towards advanced functional materials".

E. C. thanks CORIMAV ("Consortium for the Research of Advanced Materials between Pirelli and Milano Bicocca University) for its support within the PCAM European Doctoral Program.

Supplementary data

Supplementary data associated with this article can be found, in the online version, at……

References

Alexandre, M., Dubois, P., 2000. Polymer-Layered Silicate Nanocomposites: Preparation, Properties and Uses of a New Class of Materials, Mater. Sci. Eng. 28, 1-63.

Alvarez, A., 1984. Sepiolite: properties and uses. Palygorskite–Sepiolite Occurences, Genesis and Uses. In: Singer, A. Galan, E. (Eds.), Developments in Sedimentology, vol. 37. Elsevier, Amsterdam, pp. 253-287.

Akcora, P., Liu, H., Kumar, S. K., Moll, J., Li, Y., Benicewicz, B. C., Schadler, L. S., Acehan, D., Panagiotopoulos, A. Z., Pryamitsyn, V., Ganesan, V. Ilavsky, J., Thiyagarajan, P., Colby, R. H., Douglas,

J.F., 2009. Anisotropic self-assembly of spherical polymer-grafted nanoparticles, Nature Materials 8, 354-359.

Aramendía, M. A., Borau, V., Jiménez, C., Marinas, J. M., Ruiz, J. R., 1997. Characterization of Spanish sepiolites by high-resolution solid-state NMR, Solid State Nucl. Mag. 8, 251-256.

Aznar, A. J., Sanz, J., Ruiz-Hitzky, E., 1992. Mechanism of the grafting of organosilanes on mineral surfaces. IV. Phenylderivatives of sepiolite and poly (organosiloxanes), Colloid Polym. Sci. 270, 165-176.

Bandyopadhyay, A., Maiti, M., Bhowmick, A. K., 2006. Synthesis, characterisation and properties of clay and silica based rubber nanocomposites, Mater. Sci. Tech. Ser. 22, 818-828.

Breen, C., Watson, R., Madejova, J., Komadel, P., Klapyta, Z., 1997. Acid-Activated organoclays: preparation, characterization and catalytic activity of acid-treated tetraalkylammonium-exchanged smectites, Langmuir 13, 6473-6479.

Cornejo, J., Hermosin, M. C., 1988. Structural Alteration of Sepiolite by Dry Grinding, Clay Miner. 23, 391-398.

Dékány, I., Turi, L., Fonseca, A., Nagy, J. B., 1999. The structure of acid treated sepiolites: small-angle X-ray scattering and multi MAS-NMR investigations, App. Clay Sci. 14, 141–160.

D'espinose De La Caillerie, J. B., Fripiat, J. J., 1994. A reassessment of the 29Si MAS-NMR spectra of sepiolite and aluminated sepiolite, Clay Miner. 29, 313-318.

Donnet, J. B., Custodero, E., 2005. The Science and Technology of Rubber 3rd ed.; Mark, J.E.; Erman, B.; Eirich, F.R. Eds. Elsevier Academic Press Chapter 8: 367-400.

Dutta, N.K., Choudhury, N.R., Haidar, B., Vidal, A., Donnet, J.B., Delmotte, L., Chazeau, J.M., 1994. High resolution solid-state n.m.r. investigation of the filler-rubber interaction: 1. High speed 1H magic-angle spinning n.m.r. spectroscopy in carbon black filled styrene-butadiene rubber, Polymer 35, 4293-4299.

Esteban-Cubillo, A., Pina-Zapardiel, R., Moya, J. S., Barba, M. F., 2008. The role of magnesium on the stability of crystalline sepiolite structure, J. Eur. Ceram. Soc. 28, 1763-1768.

Frolich, J., Niedermeier, W., Luginsland, H. D., 2005. The effect of filler–filler and filler–elastomer interaction on rubber reinforcement, Compos Part A-Appl S. *36*, 449-460.

Galán, E., 2011. Advances in the Crystal Chemistry of Sepiolite and Palygorskite. Developments in Palygorskite–Sepiolite Research, in Developments in Clay Science. Singer, pp 281-298.

Galimberti, M., 2011. Rubber-Clay nanocomposites; Wiley.

García, N., Guzman, J., Benito, E., Esteban-Cubillo, A., Aguilar, E., Santaren, J., Tiemblo, P., 2011. Surface modification of sepiolite in aqueous gels by using methoxysilanes and its impact on the nanofiber dispersion ability, Langmuir 27, 3952-3959.

Giannini, L., Tadiello, L., Hanel, T., Galimberti, M., Cipolletti, V., Peli, G., Morazzoni, F., Scotti, R., Di Credico, B., (2015) Materiali elastomerici per componenti di pneumatici e pneumatici comprendenti fibre di silicati modificate, Filed Patent (Italy) n. MI2015A000613.

Gonzalez Hernandez, L., Ibarra Rueda, L., Chamorro Anton, C., 1987. Magnesium Silicate Filler in Rubber Tread Compounds, Rubber Chem. Technol. 60, 606-617.

Grzelczak, M., Vermant, J., Furst, E. M., Liz-Marzán, L. M., 2010. Directed self-assembly of nanoparticles, ACS Nano 4, 3591-3605.

Hakim, R.N., Hismail, H., 2008. The comparison of organoclay with respect to silica on properties of natural rubber nanocomposites, Journal of Reinforced Plastics and Composites 28, 1417-1431.

Heinrich, G., Kluppel, M., 2002. Recent advances in the theory of filler networking in elastomers, Adv. Polym. Sci. 160, 1-44.

Herrera, N.N., Letoffe, M., Reymond, J. P., Bourgeat-Lami, E., 2005. Silylation of laponite clay particles with monofunctional and trifunctional vinyl alkoxysilanes, J. Mater. Chem. 15, 863-871.

Hobbie, E. K., 2010. Shear rheology of carbon nanotube suspensions, Rheologica Acta. 49, 323-334.

Huber, G., Vilgis, T. A., 1999. Universal properties of filled rubbers: mechanisms for reinforcement on differet length scales, Kaut Gummi Kunstst 52, 102-107.

Kluppel, M., Schuster, R. H., Heinrich, G., 1997. Structure and Properties of Reinforcing Fractal Filler Networks in Elastomers, Rubber Chem. Technol. 70, 243-255.

Kojima, Y., Usuki, A., Kawasumi, M., Okada, A., Fukushima, Y., Kurauchi, T., Kamigaito, O., 1993. Mechanical properties of nylon 6-clay hybrid, J. Mater. Res. 8, 1185-1189.

Komadel, P., 1999. Natural Microporous Materials in Environmental Technology, Eds. P. Misaelides, Kluwer Academic Publishers, Dordrecht, The Netherlands, p. 3-18.

Kraus, G., 1965. In Reinforcement of Elastomers, Wiley: New York.

Krishnamoorti, R., Vaia, R.A., Giannelis, E. P., 1996. Structure and Dynamics of Polymer-Layered Silicate Nanocomposites, Chem. Mater. 8, 1728-1734.

Li, P., Wang, L., Song, G., Yin, L., Qi, F., Sun, L., 2008. Characterization of high-performance exfoliated natural rubber/organoclay nanocomposites, J. Appl. Polym. Sci. 109, 3831-3838.

Mann, S., 2009. Self-assembly and transformation of hybrid nano-objects and nanostructures under equilibrium and non-equilibrium, Nature Materials. 8, 781-792.

Miles, J.W., 2011 Amargosa Sepiolite and Saponite: Geology, Mineralogy, and Markets, Chapter 11 in Developments in Clay Science., pp 265-277.

Moenke, H. H. W., 1974. Infrared Spectra of Minerals, Eds. V. C. Farmer, Mineralogical Society, London, UK, p. 365.

Murray, H.H., 2007. Applied Clay Mineralogy: Occurrences, Processing and Application of Kaolins, Bentonites, Palygorskite-Sepiolite, and Common Clays. Elsevier, Amsterdam.

Nahmias Nanni, M., Giannini, L., Lostritto, A. 2012. High-performance tire for motor vehicle wheels comprising elastomeric material and inorganic fibers. PCT Int. Appl. WO 2012164436 A1 20121206.

Okamot, M., Nam, P.H., Maiti, P., Kotaka, T., Nakayama, T., Takada, M., Ohshima, M., Usuki, A., Hasegawa, N., Okamoto, H. 2001. Biaxial flow-indeced alignment of silicate layers in polypropylene/clay nanocomposite foam, NanoLett. 1, 503-505.

Payne, A.R., 1962. The dynamic properties of carbon black-loaded natural rubber vulcanizates. J. Appl. Polym. Sci. 6, 57-63.

Post, J. E., Bish, D. L., Heaney, P. J., 2007. Synchrotron powder X-ray diffraction study of the structure and dehydration behavior of sepiolite, Am. Mineral. 92, 91-97.

Rasband, W. S., ImageJ, U. S. National Institutes of Health, Bethesda, Maryland, USA, http://imagej.nih.gov/ij/, 1997-2016.

Ruiz-Hitzky, E., Aranda, P., Darder, M., Rytwo, G., 2010. Hybrid materials based on clays for environmental and biomedical applications, J. Mater. Chem. 20, 9306-9321.

Ruiz-Hitzky, E., Van Meerbeek, A., 2006. Developments in Clay Science. pp 583-621.

Zha, C., Wang, W., Lu, Y., Zhang, L., 2014. Constructing Covalent Interface in Rubber/Clay Nanocomposite by Combining Structural Modification and Interlamellar Silylation of Montmorillonite, ACS Appl. Mater. Interfaces. 6, 18769-18779.

Sabu, T., Ranimol, S., 2010. Rubber nanocomposites: preparation, properties and application, 1st ed.; Wiley-Interscience: New York.

Heinrich, G., Kluppel, M., Vilgis, A. T., 2002. Reinforcement of elastomers, Curr. Opin. Solid. St. M. 32, 195-203.

Scotti, R., Wahba, L., Crippa, M., D'Arienzo, M., Donetti, R., Santo, N., Morazzoni, F., 2012 Rubber–silica nanocomposites obtained by in situ sol–gel method: particle shape influence on the filler–filler and filler–rubber interactions, Soft Matter 8, 2131-2143.

Scotti, R., Conzatti, L., D'Arienzo, M., Di Credico, B., Giannini, L., Hanel, T., Stagnaro, P., Susanna, A., Tadiello, L., Morazzoni, F., 2014. Shape controlled spherical (0D) and rod-like (1D) silica nanoparticles in silica/styrene butadiene rubber nanocomposites: Role of the particle morphology on the filler reinforcing effect, Polymer 55, 1497-1506.

Susanna, A., Armelao, L., Callone, E., Dirè, S., D'Arienzo, M., Di Credico, B., Giannini, L., Hanel, T., Morazzoni, F., Scotti, R., 2015. ZnO nanoparticles anchored to silica filler. A curing accelerator for isoprene rubber composites. Chem. Eng. J. 275, 245-252.

Tadiello, L., D'Arienzo, M., Di Credico, B., Hanel, T., Matejka, L., Mauri, M., Morazzoni, F., Simonutti, R., Spirkova, M., Scotti, R., 2015. The filler–rubber interface in styrene butadiene nanocomposites with anisotropic silica particles: morphology and dynamic properties, Soft Matter 11, 4022-4033.

Vaia, R. A., Maguire, J. F., 2007. Polymer Nanocomposites with Prescribed Morphology: Going beyond Nanoparticle-Filled Polymers, Chem. Mater. 19, 2736-2751.

Valentín, L., López-Manchado, M.A., Rodríguez, A., Posadas, P., Ibarra, L., 2007. Novel anhydrous unfolded structure by heating of acid pre-treated sepiolite, App. Clay Sci. *36*, 245-255.

Valentín, J.L., López-Manchado, M.A., Posadas, P., Rodríguez, A., Marcos-Fernández, A., Ibarra, L., 2006. Characterization of the reactivity of a silica derived from acid activation of sepiolite with silane by 29Si and 13C solid-state NMR, J. Colloid Interf. Sci. 298, 794-804.

Vicente-Rodríguez, M.A., Suarez, M., Bañares-Muñoz, M.A., Lopez-Gonzalez, J.D.D., 1996. Comparative FT-IR study of the removal and structural modifications during acid silicates of octahedral cations treatment of several silicates, Spectrochim. Acta. Part A. 52, 1685-1694.

Vilgis, T.A., Heinrich, G., Klüppel, M., 2009. Reinforcement of polymer nano-composites: theory, experiments and applications. Cambridge University Press.

Weir, M.R.W., Kuang, W., Facey, G.A., Detellier, C., 2002. Solid-State nuclear magnetic resonance study of sepiolite and partially dehydrated sepiolite, Clay. Clay. Miner. 50, 240-247.

Yang, S., Yuan, P., He, H., Qin, Z., Zhou, Q., Zhu, J., Liu, D., 2012. Effect of reaction temperature on grafting of γ-aminopropyl triethoxysilane (APTES) on to kaolinite, Appl. Clay Sci. 62, 8-14.

Yebra-Rodriguez, A., Martin-Ramos, J.D., Del Rey, F., Viseras, C., Lopez-Galindo, A., 2003. A. Effect of acid treatment on the structure of Sepiolite, Clay Miner. 38, 353-360.